STEM CELLS
TRANSLATIONAL MEDICINE

Repeated injury promotes tracheobronchial tissue stem cell attrition

Moumita Ghosh[1] | Cynthia L. Hill[2] | Alfahdah Alsudayri[2] | Scott W. Lallier[2] | Don Hayes Jr.[3] | Saranga Wijeratne[3] | Zhang Hong Tan[4] | Tendy Chiang[4] | John E. Mahoney[5,6] | Gianni Carraro[7] | Barry R. Stripp[7] | Susan D. Reynolds[2,3]

[1]Department of Medicine, University of Colorado-Denver, Denver, Colorado, USA

[2]Center for Perinatal Research, Nationwide Children's Hospital, Columbus, Ohio, USA

[3]Department of Pediatrics, The Ohio State University College of Medicine, Columbus, Ohio, USA

[4]Center for Regenerative Medicine, Nationwide Children's Hospital, Columbus, Ohio, USA

[5]Cystic Fibrosis Foundation Therapeutics, Lexington, Massachusetts, USA

[6]Cystic Fibrosis Foundation, Bethesda, Maryland, USA

[7]Department of Medicine, Cedars-Sinai Medical Center, Lung and Regenerative Medicine Institutes, Los Angeles, California, USA

Correspondence
Susan D. Reynolds, PhD, Nationwide Children's Hospital, 700 Children's Drive, Columbus, OH 43205, USA.
Email: susan.reynolds@nationwidechildrens.org

Abstract

Chronic lung disease has been attributed to stem cell aging and/or exhaustion. We investigated these mechanisms using mouse and human tracheobronchial tissue-specific stem cells (TSC). In mouse, chromatin labeling and flow cytometry demonstrated that naphthalene (NA) injury activated a subset of TSC. These activated TSC continued to proliferate after the epithelium was repaired and a clone study demonstrated that ∼96% of activated TSC underwent terminal differentiation. Despite TSC attrition, epithelial repair after a second NA injury was normal. The second injury accelerated proliferation of previously activated TSC and a nucleotide-label retention study indicated that the second injury recruited TSC that were quiescent during the first injury. These mouse studies indicate that (a) injury causes selective activation of the TSC pool; (b) activated TSC are predisposed to further proliferation; and (c) the activated state leads to terminal differentiation. In human TSC, repeated proliferation also led to terminal differentiation and depleted the TSC pool. A clone study identified long- and short-lived TSC and showed that short-lived TSC clones had significantly shorter telomeres than their long-lived counterparts. The TSC pool was significantly depleted in dyskeratosis congenita donors, who harbor mutations in telomere biology genes. The remaining TSC had short telomeres and short lifespans. Collectively, the mouse and human studies support a model in which epithelial injury increases the biological age of the responding TSC. When applied to chronic lung disease, this model suggests that repeated injury accelerates the biological aging process resulting in abnormal repair and disease initiation.

KEYWORDS
airway epithelial stem cell, basal cell, biological aging, chronic lung disease

Significance statement

Results of the present study identify biological aging as an important aspect of tracheobronchial tissue-specific stem cell phenotype and function and one that could impact the development of chronic lung disease.

1 | INTRODUCTION

Age has two components. Chronological age is the number of years since birth. In contrast biological age accounts for external factors which modify function. Accordingly, biological age can differ from chronological age and discordance has been detected in whole organisms as well as individual cells. In two chronic lung diseases, idiopathic pulmonary fibrosis (IPF) and chronic obstructive pulmonary disease (COPD), the biological age of lung cells is greater than their chronological age.[1,2] While these studies identified accelerated aging as a novel pulmonary disease process, translational initiatives require a better understanding of chronological aging and the factors that increase biological age.

A tissue-specific epithelial stem cell is defined as an epithelial cell that replaces itself and acts as a progenitor for each of the specialized epithelial cell types that are found in the stem cell's trophic unit. These properties are controlled by intrinsic processes that are subject to regulation by niche-derived extrinsic signals. Several studies indicate that tissue-specific stem cell self-renewal and multilineage differentiation declines over time and that these changes decrease regenerative capacity.[3] This loss of function, which is an indication of aging, may cause the tissue-specific stem cell and its home tissue to be biologically older than its chronological age. In IPF and COPD, aging was detected across lung cell types and led to the idea that many types of tissue-specific stem cells were biologically older than their chronological age.[1,2]

Conducting airway epithelial remodeling is a hallmark of many chronic lung diseases, including cystic fibrosis, asthma, COPD, and IPF.[4] In these diseases, repeated injury and aberrant repair alter the frequency of differentiated airway epithelial cells (reviewed in[2,5]). The resulting epithelial remodeling has been attributed to stem/progenitor cell aging and/or exhaustion. However, the underlying mechanism, including whether loss of function is due to intrinsic and/or extrinsic factors, is unclear.

This study examined biological aging of the tracheobronchial epithelial tissue-specific stem cell (TSC). TSC regenerate the pseudostratified airway epithelium and reside in the tracheobronchial regions of the mouse and human upper respiratory tract. Clonal analysis in human[6] and lineage-tracing in mice[7-10] indicated that the TSC was a basal cell subtype which generated basal, ciliated, secretory epithelial cells, and a variety of rare epithelial cell types.

We previously used in vitro clonal analysis to investigate the intrinsic behavior of TSC and avoid the confounding variables associated with their niche. These studies demonstrated that mouse TSC generated a specific clone type, the rim clone, in vitro.[11] Serially passaged TSC terminated when they generated a unipotential basal (UPB) cell, which was the last clone forming TSC descendant. The TSC-to-UPB transition was indicated by formation of UPB-derived non-rim clones. Our previous studies demonstrated that the terminal differentiation process was driven by repeated cell division.[11-13] Collectively, these studies challenged the idea that the TSC maintains its function throughout an individual's life and suggested a cell-intrinsic proliferation-based biological aging mechanism.

Biological aging, particularly at the cellular level, has been associated with telomere shortening.[3] Telomeres are 6 base pair repeats that are generated by the reverse transcriptase telomerase (TERT) and form the ends of chromosomes. Mouse telomeres are ∼200 kilobases (kb) in length; whereas, human telomeres are ∼25 to 50 kb.[14] Consequently, telomere length studies are frequently conducted in human.

Telomeres prevent loss of genetic information during DNA replication.[3] In parallel, the shelterin protein complex interacts with telomere repeats and prevents recognition of the single-stranded chromosome end as a double-strand break. Most mammalian somatic cells express little or no TERT, consequently telomeres shorten as the cells divide in response to normal cell turnover or injury-induced cell death. In vivo and in vitro studies demonstrated that telomere length was inversely correlated with biological age and that critically short telomeres led to a decrease in stem cell frequency.[3]

Dyskeratosis congenita (DC) is a disease of premature aging that is caused by mutations in telomere biology genes.[15] Most disease-causing mutations (TERT, TERC, DKC1, NOP10, NHP2, TPP1, WRAP53) compromise TERT/TERC dependent telomere lengthening. In contrast, mutation of TINF2 and CTC1 prevent assembly of the shelterin complex and allow telomere ends to be detected by the DNA damage pathway.

Although DC is a multisystem disorder, patients typically present with nail dystrophy, changes in skin pigmentation, and oral leukoplakia. Many conditions with prominent cutaneous findings also have significant pulmonary manifestations[16] and ∼20% of DC patients develop usual interstitial pneumonia which is a form of pulmonary fibrosis (reviewed in Reference 17). Like IPF and COPD, fibrotic lesions in DC involve both the bronchial and alveolar regions. Fibrosis in DC patients may overlap with pulmonary arteriovenous malformations which are a recently recognized and common feature of DC-lung disease.[17] The most severe forms of DC lead to bone marrow failure and analysis of telomere length in leukocytes from DC patients associated telomere shortening with hematopoietic stem cell attrition. The multisystem nature of DC and presence of pulmonary disease suggested that telomere biology gene mutations might alter TSC number or lifespan.

This project evaluated biological aging in mouse and human TSC. Based on the association between TSC proliferation and terminal differentiation, we used single and repeated injuries to determine the impact of TSC proliferation on lifespan. In mice, naphthalene (NA) exposure was used to model injuries that result in epithelial cell death. TSC mitotic frequency was quantified in vivo using chromatin and nucleotide labeling. Terminal differentiation was quantified in TSC clones that were serially passaged in vitro. As previously reported for analysis of hematopoietic stem cell number and lifespan,[18] serial passage of human TSC from normal and DC donors was used to model the cell death and decreased epithelial cell density which are characteristic of epithelial injury. Human TSC number, lifespan, differentiation potential, and telomere length were quantified.

2 | MATERIALS AND METHODS

2.1 | Human and mouse study approvals

The Institutional Review Board at Nationwide Children's Hospital approved the human studies. Written informed consent and assent

was obtained from every participant. All procedures involving animal use were approved by the Institutional Animal Care and Use Committee at National Jewish Health or Nationwide Children's Hospital. Mice were maintained in AAALAC-approved facilities and screened quarterly for pathogens.

2.2 | Mouse models

NA was prepared and administered by intraperitoneal injection as previously reported.[19] NA dose was selected to cause >95% depletion of the Clara cell secretory protein (CCSP) positive cell population by recovery day 3. The Keratin 5-reverse tetracycline trans-activator/ tetracycline responsive element-Histone 2B:green fluorescent protein (K5-rtTA/TRE-H2B:GFP) chromatin-labeling model facilitates purification of basal cells that proliferate frequently or infrequently after injury.[20] Male and female K5-rtTA[21]/TRE-H2B were used for the label-retention studies. Mice were fed doxycycline chow and treated with 250 mg/kg NA as detailed in Results. Female FVB/n mice, 6 to 8 weeks old, were treated with 300 mg/kg NA. Groups of mice were treated with 50 mg/kg Bromodeoxyuridine BrdU and/or 42 mg/kg 5-ethynyl-2′-deoxyuridine (EdU) as detailed in Results.

2.3 | Immunofluorescence studies

Tracheal tissue sections (5 μm) were generated from paraffin-embedded tissues and processed as described previously.[22] All antibodies (K5, CCSP, BrdU, and ACT), and staining methods were previously described.[19] EdU was detected using the ClickIt method and followed the manufacturer's instructions. Images were acquired using an upright Zeiss Imager Z1 fluorescent microscope and AxioVision software (Carl Zeiss) or an inverted Zeiss 200 M confocal microscope using Intelligent Imaging Innovations Inc. software. Cell type frequency was quantified as previously indicated[22] and values were expressed as a percent of total epithelial cells. N = 6 tracheas/group.

2.4 | Mouse TSC quantification

Tracheal epithelial cells were recovered by dispase/collagenase/trypsin (DCT) digestion and clone forming cell frequency (CFCF) was determined by limiting dilution.[11] Mouse cells were plated on irradiated NIH3T3 (ATCC #CRL-1658) feeder layers and cultured in mouse tracheal epithelial medium (MTEC+,[23]). On culture day 10, the cells were fixed and stained with Geimsa. TSC clones were identified as previously reported.[11] Time points are noted in Results.

2.5 | Mouse flow cytometry

Tracheal epithelial cells were recovered by digestion with DCT. A Moflo high-speed cell sorter (Dako Cytomation) was used to identify:

(a) cells that were CD45-/CD31−/TER119-/DAPI-; (b) quantify GFP-fluorescence intensity in each cell; and (c) to separate CD49f+/Sca1+ cells into GFP[bright] and GFP[dim] subsets.

2.6 | Mouse serial passage analysis

Passage (P) 0 TSC clones were derived from NA treated mice that had been recovered 40 days. One thousand tracheal epithelial cells were plated in each well of a 6-well plate that contained an irradiated NIH3T3 fibroblast feeder cell layer. The cells were cultured in MTEC+ medium for 10-days. TSC clones were identified by their characteristic rim morphology and isolated at each passage using cloning cylinders as previously reported.[11] This process was repeated with P1-P4 TSC-clones. At P5, the number of cells/clone and the TSC- and UPB-CFCF were used to calculate the number of TSC and UPB derived clones.

2.7 | Gene expression analysis

Quantitative reverse transcription polymerase chain reaction (qRT-PCR) methods and Assays-on-Demand probe primer pairs were as previously reported.[13] Single Cell RNA sequencing (scRNAseq) was done at the Ohio State University Shared Genomics Resource and used the 10XGemomics platform. Analytical methods are detailed in the supplement.

2.8 | Human TSC recovery, culture, and enumeration

Human bronchial and nasal TSC were recovered as previously described.[24,25] Normal donor demographics were described previously.[24] DC donor demographics are presented in Table S1. The modified conditional reprogramming culture (mCRC) method[25] was adapted from Suprynowicz et al.[26] The major change from this protocol was the use of irradiated NIH3T3 fibroblast feeder layers. Differentiation was evaluated in air-liquid-interface cultures and quantified as previously described.[25] The CFCF assay[11] was used to determine TSC number.

2.9 | Telomere length determination

Genomic DNA was purified using the DNeasy Blood & Tissue Kit (69506, Qiagen); 40 ng of gDNA was used for telomere and 36B4 single copy gene control assays. Targets were amplified using previously reported standards and primers.[27] Previously published cycling parameters for telomeres[28] and 36B4[27] were used. Magnesium concentration in the PowerSYBR Green Master Mix (Applied Biosystems 4367659) was lowered through the addition of 0.5 M EDTA (0.0385 μL per 20 μL reaction for a final concentration of 0.9625 mM) for the telomere assay.[28] Jurkat (ATCC) and U1301 (human T-cell leukemia cell line (01051619, Sigma) were used as short and long

telomere controls, respectively. A standard curve was generated for each experiment and was used to insure a linear relationship between DNA input and telomere length. Three technical replicates were generated for each standard curve point and biological sample. Relative telomere length was calculated according to the Telomere/Single copy gene control (T/S) ratio.[27]

2.10 | Statistical analyses

All statistical analyses were performed using Graph Pad Prism. Data normality was evaluated by the Shapiro-Wilk test, the Anderson-Darling test, and/or the D'Agostino & Pearson test. For normally distributed data sets, differences were evaluated using Student's t-test. For non-normally distributed data sets, differences were evaluated by the Mann-Whitney test and data are presented as the median and the interquartile range. Trends were analyzed by regression analysis. The definition of center and dispersion precision measures are indicated in the figure legends. Data sets containing multiple variables were analyzed by analysis of variance (ANOVA) and a post hoc Tukey test (normally distributed data sets) or Kruskal Willis test (non-normally distributed data sets). Sample size is indicated in the figure legends. P-values <.05 were considered significant.

3 | RESULTS

3.1 | TSC continue to proliferate after the epithelium is repaired

Tissue-specific stem cells are typically characterized as cells that divide infrequently. This property is demonstrated by retention of a chromatin or DNA label.[20] In this study, the chromatin labeling approach was used to determine the mitotic frequency of TSC 6 to 80 days after a single NA exposure. K5/H2B:GFP mice and mono-transgenic controls were fed Dox chow for 3 days, treated with NA on day 0, and switched to standard chow on day 3 (Figure 1A). Mice were recovered to day 6, 40, or 80. Flow cytometry was used to evaluate GFP fluorescence intensity (Figure 1B). The frequency of GFP-Bright, -Dim, and -Negative cells within the CD49f-Bright/Sca1+ basal cell population was quantified across three experiments (Figure 1C-E).

The frequency of GFP-bright cells decreased significantly between days 6 and 40 but did not change between days 40 and 80 (Figure 1F). The frequency of GFP-Dim cells did not vary as a function of time (Figure 1G). However, the frequency of GFP-Negative basal cells was significantly increased on days 40 and 80 (Figure 1H). These data indicated that a single NA injury generated a GFP-Bright population and that most of these cells proliferated by 80.

A previous study reported that a 2-fold decrease in GFP mean fluorescence intensity (MFI) occurred with each cell division.[29] The MFI was 6×10^4 for GFP-Bright cells, 5×10^3 GFP-Dim cells, and 4×10^3 for GFP-Negative cells (Figure 1B). These data indicate that many GFP-Bright cells divided ~3 times between days 6 and 40 and another 3 times between days 40 and 80. Knowing that the tracheal epithelium is repaired within 13 days of NA injury[19] and that most GFP-Bright cells are TSC[13] these data indicated that TSC continued to proliferate after the epithelium was repaired.

3.2 | A second injury accelerates TSC proliferation

The previous study indicated that a subset of TSC retained the GFP label to day 40. To determine if these cells proliferated in response to a second injury, K5/H2B:GFP mice and controls were fed Dox chow between days −3 and + 3 and treated with NA on day 0. The mice were recovered to day 40 (Figure 2A). A second group of mice was retreated with NA on day 40 and recovered to day 80 (Figure 2B). Flow cytometry was used to evaluate GFP fluorescence 40 days after the first or second injury (Figure 2C,D).

The frequency of GFP-Bright cells did not change significantly in response to the second injury (Figure 2E). However, the MFI for GFP-Bright cells decreased (compare Figure 2C,D). The frequency of GFP-Dim cells (Figure 2F) was significantly decreased after the second injury and the frequency of GFP-Negative cells increased (Figure 2G). This analysis indicated that GFP-Bright cells proliferated in response to the second injury and that the second injury accelerated the proliferation of TSC within the GFP-Dim population. These data suggested that the initial injury/repair process generated a pool of "activated" TSC which were predisposed to proliferate in response to the second injury.

3.3 | Terminal differentiation depletes the TSC pool

In contrast with the idea that TSC proliferate and then exit the cell cycle, results from the first two studies indicated that activated TSC continued to proliferate. Since our previous studies demonstrated that TSC have a finite lifespan and that proliferation in vivo or in vitro promoted terminal differentiation to a UPB cell,[11,13] we hypothesized that TSC clones from injured mice would generate fewer TSC than UPB. TSC clones were isolated from K5/H2B:GFP mice were treated with NA as indicated (Figure 1A). On day 40, nine TSC were recovered, cloned, and serially passaged. This study demonstrated that 100% of TSC recovered from NA-injured mice survived at least three passages (Figure 3A). A similar analysis of sixteen TSC from uninjured mice also demonstrated 100% survival to passage 3 (Figure 3B).

To determine the fate of TSC at passage 3, the clone forming cell frequency (CFCF) assay was used to determine the frequency of rim (TSC-derived clones) and non-rim (UPB-derived clones). TSC from injured mice formed two subsets: 62% of clones generated more TSC than UPB, whereas 38% of clones generated fewer TSC than UPB (Figure 3C). In contrast, most TSC from uninjured mice (88%) produced equal numbers of TSC and UPB (Figure 3D).
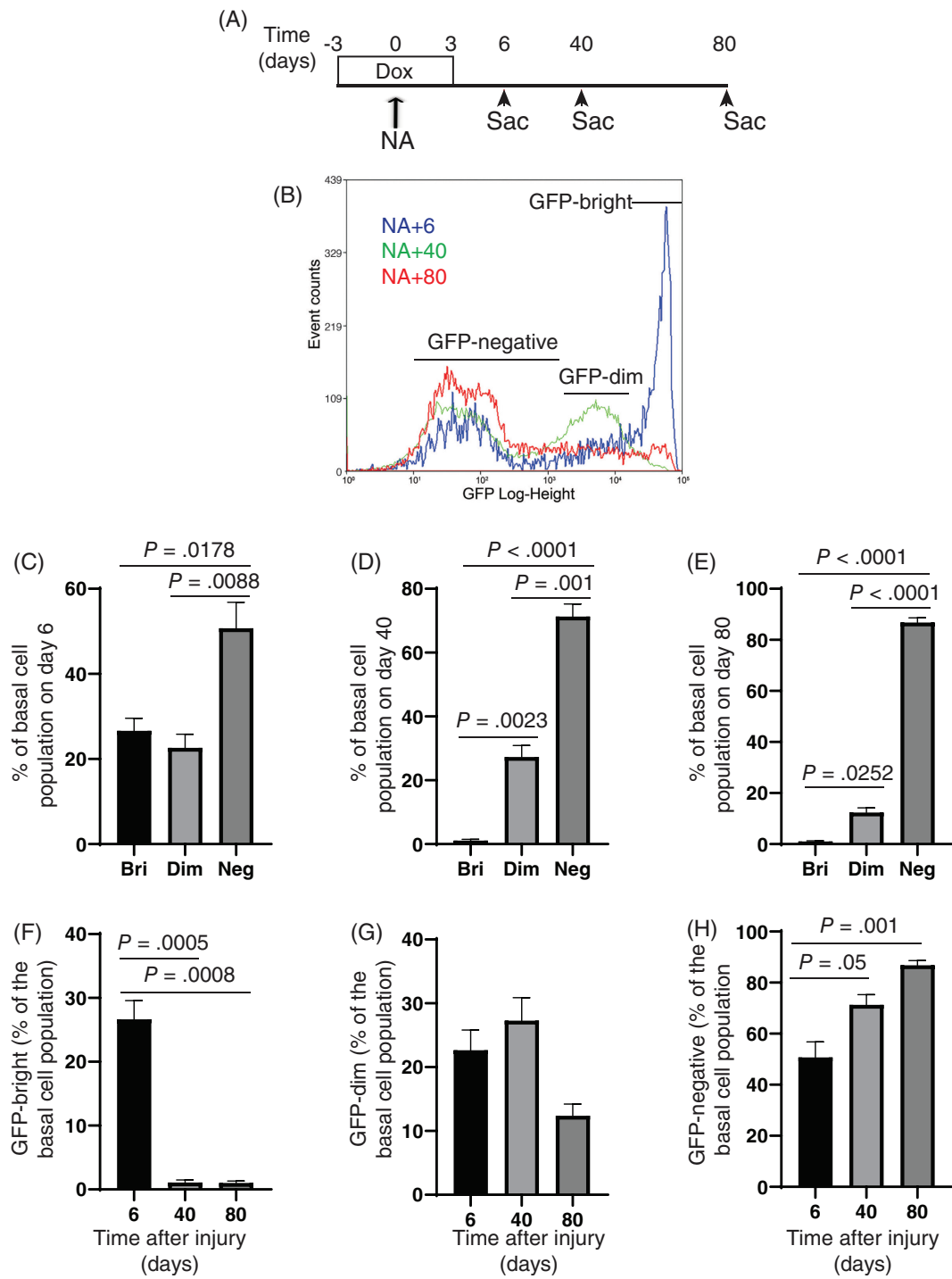
FIGURE 1   Analysis of TSC cell cycle frequency after a single NA injury. A, Experimental design. K5/H2B:GFP mice and mono-transgenic controls were treated with Dox chow from day −3 through day +3 and then switched to standard chow. NA treatment occurred on day 0. Animals were euthanized (Sac) on days 6, 40, and 80. B, Representative flow cytometric analysis of green fluorescent protein (GFP) fluorescence intensity. C-E, Frequency of GFP-Bright (Bri), GFP-Dim, and GFP-Negative (Neg) cells on days 6 (C), 40, (D), and 80 (E). D-F, Frequency of GFP-Bri (F), GFP-Dim (G), and GFP-Neg (H) a function of time after injury. Mean ± SEM (n = 3)

The finding that TSC from uninjured mice generated UPB indicated that terminal differentiation was not unique to activated TSC. However, the injury-associated skewing of TSC fate was unexpected. To examine this process, we serially passaged TSC clones 1 and

2 which generated significantly more TSC clones than UPB cell clones and TSC clones 3 and 4 which generated significantly fewer TSC clones than UPB cell clones. Clone 4 was not evaluated because it terminated at passage 3.
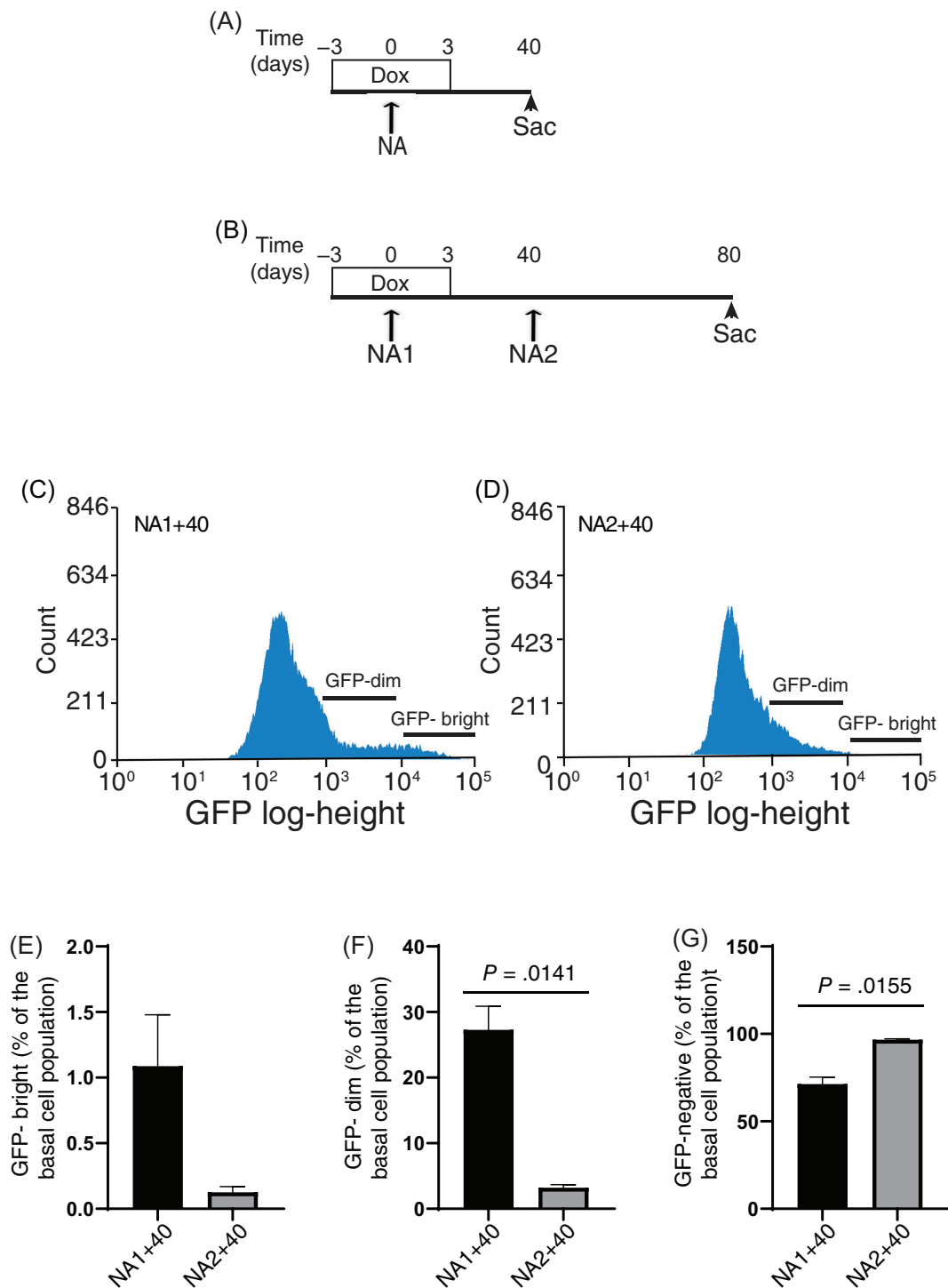
FIGURE 2 Analysis of TSC cell cycle frequency after a second NA injury. A,B, Experimental design. K5/H2B:GFP mice and mono-transgenic controls were treated with Dox chow from day −3 through day +3 and then switched to standard chow. NA treatment occurred on day 0. Animals were euthanized (Sac) on day 40 (A). Mice were treated as indicated above (NA1) and retreated with NA on day 40 (NA2). Mice were euthanized on day 80 (B). C,D, Flow cytometry was used to evaluate green fluorescent protein (GFP) fluorescence intensity 40 days after NA1 (C) or NA2 (D). Representative of three biological replicates. E, Frequency of GFP-Bright cells 40 days after NA1 or NA2. F, Frequency of GFP-Dim cells 40 days after NA1 or NA2. G, Frequency of GFP-Negative cells 40 days after NA1 or NA2. Mean ± SEM (n = 3)

To further evaluate the behavior of TSC, limiting dilution was used to generate clonal sublines from the three long-lived TSC clones (clones 1-3). The clone-1 sublines generated only TSC clones at P4 (Figure 4A). Sub-cloning generated 40 clones at P5 (Figure 4B). Two of the P5 sub-clones (5%) generated only TSC clones; whereas, the remaining 38 clones (95%) generated a mixture of TSC and terminally

differentiated UPB clones. Each of the mixed sub-clones generated more TSC clones than UPB clones.

Clone-2 sublines generated both TSC and UPB clones at P4 (Figure 4C). Sub-cloning of 31 TSC identified 29 clones (94%) that survived to P5 (Figure 4D). Among the surviving TSC clones, 2 (6.9%) generated only TSC, 14 (48%) generated fewer TSC clones than UPB clones, and 12 (41%) generated only UPB clones.

Three clone-3 sublines generated only TSC clones at P4, while the fourth subline generated both TSC and UPB clones (Figure 4E). Sub-cloning of 28 TSC identified 27 clones (96%) that survived to P5 (Figure 4F). Seven of these clones (26%) generated both TSC and UPB clones; whereas 18 clones (67%) generated only UPB.

This analysis demonstrated that only 4.3% of TSC clones self-renewed at P5 and that the vast majority of TSC had entered the terminal differentiation pathway. Since our previous study suggested a role for WNT signaling in TSC cell fate decisions,[13] we used qRT-PCR to examine this mechanism in TSC subclones at passage 5 (Figure S1). This study identified a unique gene expression signature for clone 1 subclones. However, additional studies are needed to delineate a molecular mechanism. Collectively, these studies indicated that repeated proliferation and terminal differentiation depleted the activated TSC pool.

3.4 | Comparable TSC proliferation within 6 days of the first and second NA injuries

TSC depletion suggested that injury might compromise reparative potential. To address this issue, we compared the mitotic frequency of TSC after the first and second NA exposures. Group 1 consisted of K5/H2B:GFP mice and controls which were fed Dox chow for 3 days, treated with NA on day 0, switched to standard chow on day 3, and recovered to day 6 (Figure 5A). Group 2 consisted of K5/H2B:GFP mice and controls which were treated with NA on day 0, switched to Dox chow on day 37, retreated with NA on day 40, switched to standard chow on day 43, and recovered to day 46 (Figure 5B). Analysis of GFP fluorescence demonstrated that group 2 contained GFP-bright cells and that the pattern of GFP fluorescence was indistinguishable from that observed in group 1 (Figure S2A). Flow analysis of epithelial cell phenotype in groups 1 and 2 did not detect differences in the frequency of epithelial, basal, GFP-Dim, or GFP-Bright cells (Figure 5D). These data indicate that the early TSC response to the first and second injuries were similar.

3.5 | Divergent TSC proliferation 40 days after the first and second NA injuries

To compare TSC mitotic frequency at later time points, we evaluated GFP fluorescence and cell phenotype 40 days after the first or the second NA injury. Group 3 mice were treated with Dox and NA as indicated for croup 1 and were recovered to day 40 (Figure 5A). Group 4 mice were treated with Dox and NA as indicated for group

2 and were recovered to day 80 (Figure 5B). Analysis of GFP fluorescence and epithelial phenotype demonstrated that group 3 had significantly more CD49f-Bright/Sca1+ cells than group 4 and that group 3 had significantly fewer GFP-Bright cells than group 4. These data indicated that group 3 cells proliferated more frequently than group 4 cells.

The previous study suggested that two mitotically distinct populations of TSC were involved in epithelial repair. To evaluate this idea, we compared GFP fluorescence and cell phenotype in group 4 mice with K5/H2B:GFP mice and controls which were fed Dox chow for 3 days, treated with NA on day 0, switched to standard chow on day 3, retreated with NA on day 40, and recovered to day 80 (group 5, Figure 5C). Analysis of GFP fluorescence showed distinct profiles for groups 4 and 5 (Figure S2B). Quantification demonstrated that the frequency of epithelial and basal cells did not differ for groups 4 and 5 (Figure 5F). However, the frequency of GFP-Dim and GFP-Bright cells was significantly decreased in group 5 relative to group 4. These data further supported the idea that cells labeled during the first injury continued to proliferate after the second injury and raised the possibility that the second injury activated a distinct cohort of TSC.

3.6 | The second injury activates a new cohort of TSC

To determine if the same set of TSC responded to the first and second injuries, we used the nucleotide label-retention technique. Mice were treated with NA on day 0 and mitotic cells were labeled with BrdU (Figure 6A, upper panel). The frequency of BrdU label-retaining cells was assayed on days 40 and 80. Another group of mice was reinjured and mitotic cells were labeled with EdU (Figure 6A, lower panel). The frequency of EdU+, BrdU+, and BrdU+/EdU+ label-retaining cells was assayed on day 80.

Histological analysis (Figure 6B-D) and quantification demonstrated that the frequency of BrdU+ cells decreased significantly between days 40 and 80 (Figure 6E). These data are consistent with the chromatin labeling studies (Figure 2) and indicate that many BrdU-tagged cells proliferated in response to the second injury. On Day 80, the frequency of EdU+ cells was significantly greater than the frequency of BrdU+ and BrdU+/EdU+ cells and the frequency of BrdU+ and BrdU+/EdU+ cells was similar (Figure 6F). Furthermore, the frequency of EdU+ cells within the label-retaining cell population was significantly greater than that of the BrdU+ or BrdU+/EdU+ populations (Figure 6G). These data supported the idea that the second injury activated a new cohort of TSC.

3.7 | Telomere shortening in serially passaged human TSC

TSC depletion in mice resembled the loss of clone forming cells in serially-passaged human TSC,[24] (Figure 7A) and raised the possibility
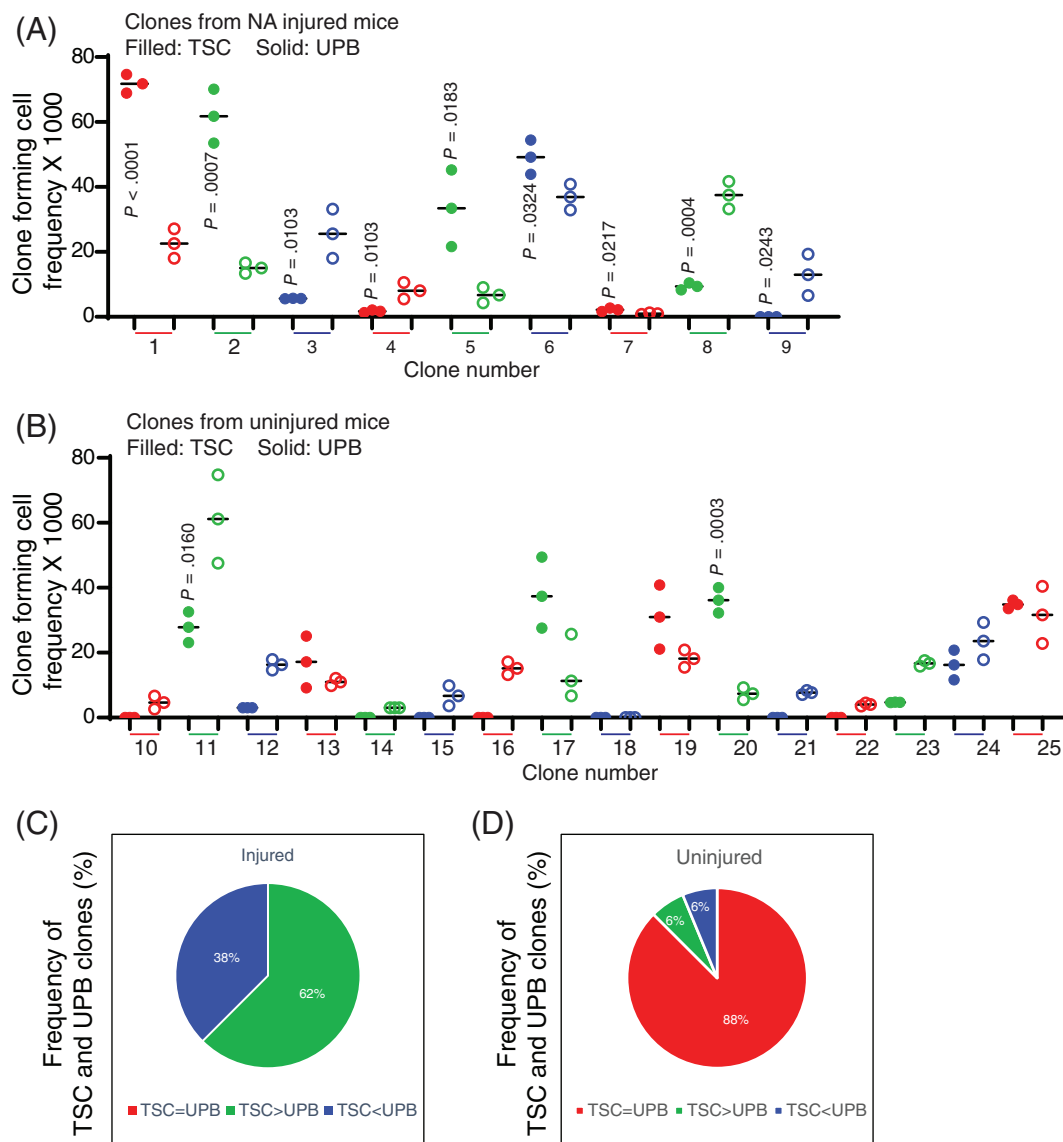
FIGURE 3 Lifespan and fate analysis of TSC clones. A, K5/H2B:GFP mice and mono-transgenic controls were treated with dox chow from day −3 through day +3 and then switched to standard chow. NA treatment occurred on day 0. On day 40, TSC were recovered, cloned, and serially passaged. TSC (filled symbols) and UPB (open symbols) clone forming cell frequency (CFCF) for nine TSC clones at passage 3. B, TSC were recovered from uninjured K5/H2B:GFP mice. CFCF was determined for 16 TSC clones at passage 3. Symbols are as indicated above. C, Fate of TSC clones from injured mice. D, Fate of TSC clones from uninjured mice

that short-lived TSC had proliferated repeatedly prior to isolation. Since proliferation of somatic cells and TSC attrition has been associated with telomere shortening,[30] we used PCR to determine telomere length in serially passaged human TSC. This study demonstrated that telomeres shortened as a function of passage (Figure 7B). To determine if serial passage was selecting TSC with relatively long telomeres, human TSC were cloned at P3 and telomere length was determined for the parental populations and clonal isolates at P4-P11. Telomere length was significantly greater in clones than in populations at P4 to P6 (Figure 7C). These data indicate that short-lived TSC enter culture with relatively short

telomeres and that a further decrease in telomere length contributes to TSC attrition over P1 through P5.

The telomere length study also found that telomere length was stable, but short, at later passages (Figure 7C). To determine if long-lived TSC expressed telomere maintenance genes TERT and TERC, we used RNAseq to evaluate expression of these genes as a function of time after plating. This study did not detect TERT or TERC mRNA at any time point (Figure 7D) and was in agreement with other studies which did not detect TERT gene expression or function.[25,31] However, TERT activity has been reported in TSC[26,32] and it was possible that these population studies may have overlooked TERT and TERC
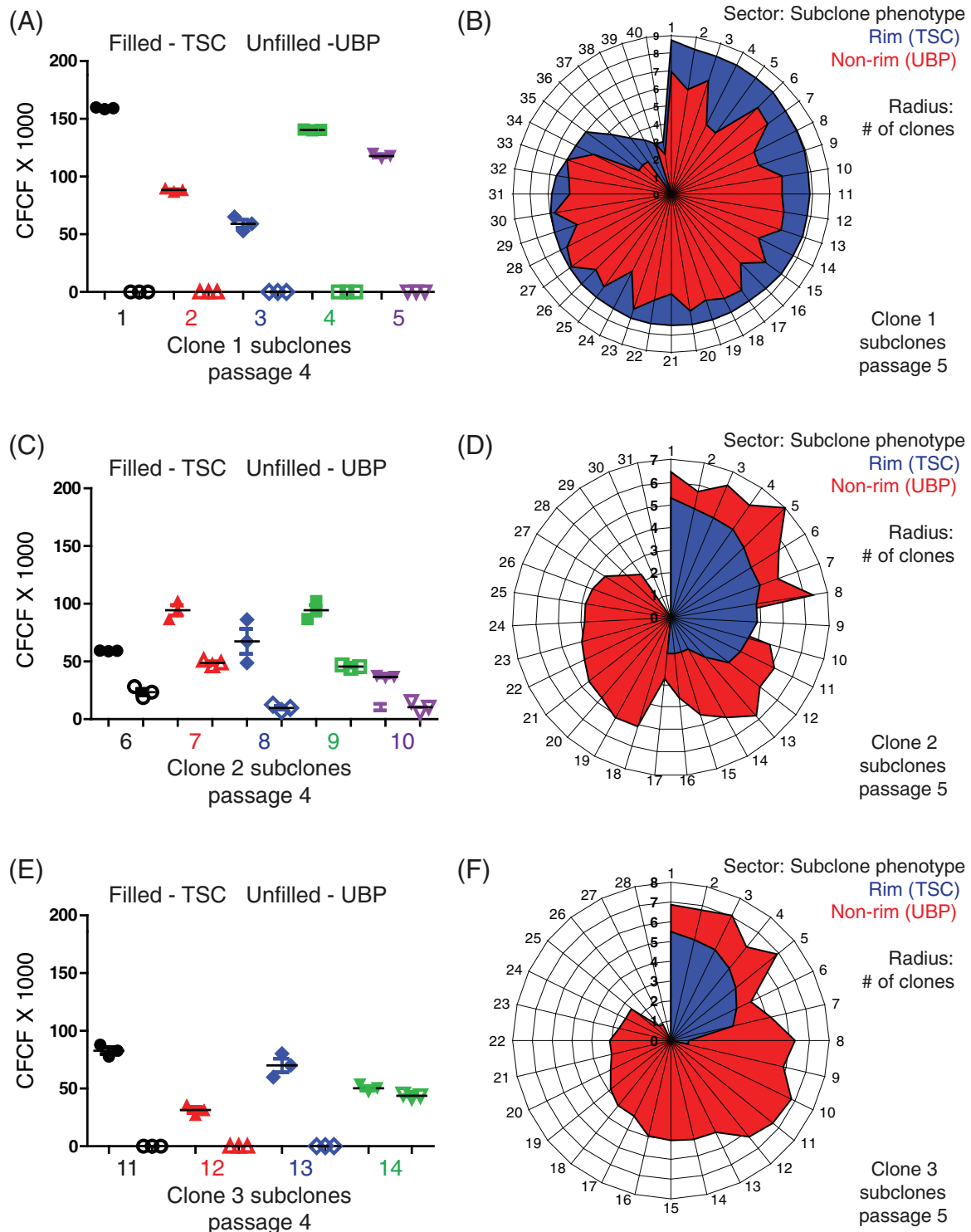
FIGURE 4 Fate analysis of long-lived TSC clones. TSC clones 1 to 3 were subcloned at passages 3 and 4. A,B, Clone 1, subclones 1 to 5. C,D, Clone 2, subclones 6 to 10. E,F, Clone 3, subclones 11 to 14. A,C,E, TSC (filled symbols) and UPB (open symbols) clone forming cell frequency (CFCF) analysis for subclones at passage 4. B,D,F, The number of TSC and UPB subclones per TSC clone at passage 5. Sectors represent subclones. Diameter represents the number of TSC (blue) or UPB (red) clones

expression in a rare subpopulation. To address this issue, we queried a scRNAseq data sets for expression of telomere biology genes.[3] Analysis of freshly isolated human lung cells as well as TSC that were

proliferating in vivo did not detect a TERT- or TERC-expressing subpopulation (Figure S3). Collectively, these data indicate that TSC do not express TERT or TERC.
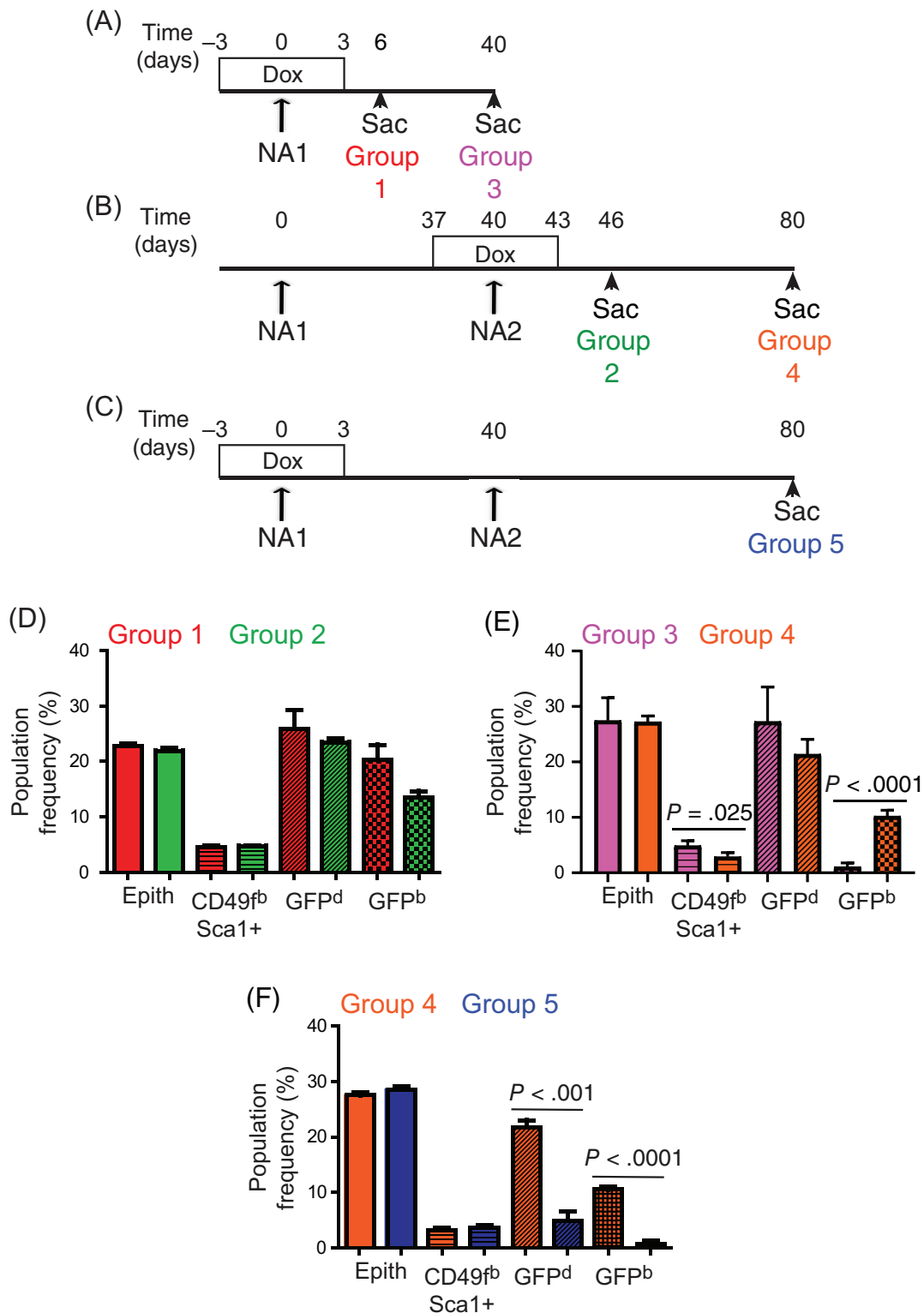
FIGURE 5 Comparison of the TSC response to a single or repeated NA injury. A-C, Experimental design. All studies used K5/H2B:GFP mice and mono-transgenic controls. Mice were treated with Dox chow from day -3 through day $+3$ and then switched to standard chow. NA treatment occurred on day 0. Animals were euthanized (Sac) on days 6 (group 1) or 40 (group 3) (A). Mice were treated with NA on day 0, fed Dox chow from days 37 to 43, and retreated with NA on day 40 (NA2). Mice were euthanized on days 46 (group 2) and 80 (group 4) (B). Mice were treated with Dox and NA as indicated in panel A and retreated with NA on day 40 (NA2), and recovered to day 80 (group 5) (C). D, Frequency of epithelial (Epith), basal cells (CD49f^b/Sca1$^+$), GFP-Dim (GFP^d), and GFP-Bright (GFP^b) cells in Groups 1 and 2. The frequency of each subset within the CD45-/CD31−/TER119-/DAPI- population was determined. Mean ± SEM (n = 3). E, Frequency of Epith, CD49f^b/Sca1$^+$, GFP^d, and GFP^b cells in Groups 3 and 4. Mean ± SEM (n = 3). F, Frequency of Epith, CD49f^b/Sca1$^+$, GFP^d, and GFP^b cells in Groups 4 and 5. Mean ± SEM (n = 3)
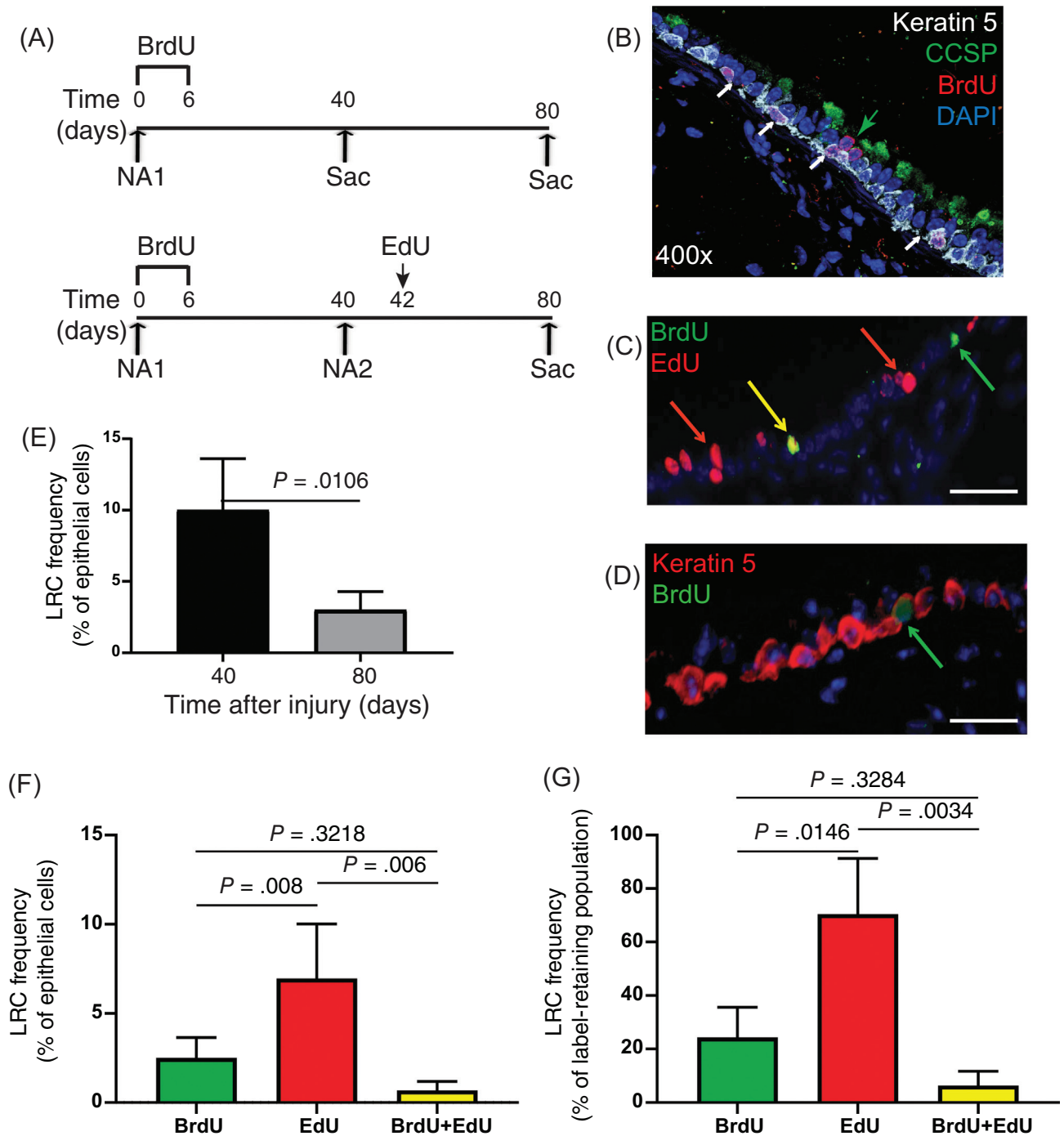
FIGURE 6 Nucleotide label retention analysis of TSC that proliferate after the first and second NA injuries. A, Experimental design. Top panel: FVB/n mice were treated with NA on day 0 and Bromo-deoxyuridine (BrdU) on days 0 to 6. Tissue was recovered on day 40 (sac). Bottom panel: Mice were treated as indicated in the top panel (NA1) and retreated with NA on day 40 (NA2). Mice were treated with 5-ethynly-2′-deoxyuridine (EdU) on day 42. Tissue was recovered on day 80. B, Histological analysis of Keratin 5 (white), CCSP (green), BrdU (red), and DAPI (blue) 40 days after NA injury. White arrows indicate Keratin 5/BrdU+ cells. C, Histological analysis of BrdU (green) and EdU (red) on day 80. Green arrow indicates a BrdU+ cell. Red arrows indicate EdU positive cells. Yellow arrow indicates a BrdU/EdU positive cell. Scale bar, 50 μm. D, Histological analysis of Keratin 5 (red) and BrdU (green) on day 80. Green arrow indicates a Keratin 5/BrdU double-positive cell. Scale bar, 50 μm. E, Frequency of BrdU label retaining cells (LRC) within the epithelial cell population on recovery days 40 and 80. F,G, Quantification of BrdU+, EdU+, and BrdU+/EdU+ LRC on day 80. F, Frequency of BrdU+, EdU+, and BrdU+/EdU+ LRC as a percentage of all epithelial cells. G, Frequency of BrdU+, EdU+, and BrdU+/EdU+ LRC as a percentage of the label-retaining cell population. E-G, Mean ± SEM (n = 3-5)
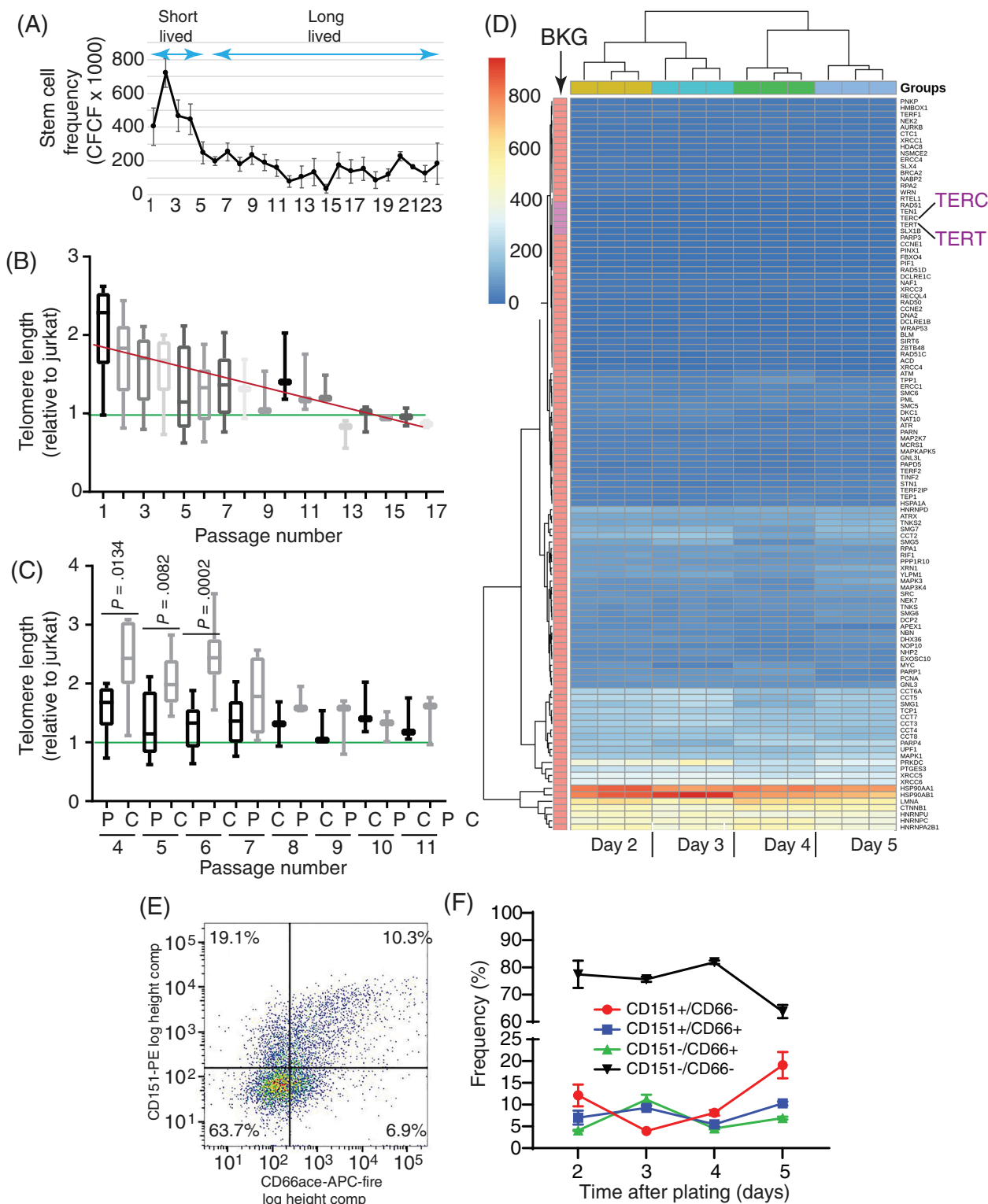
FIGURE 7   Telomere length and secretory differentiation in human TSC. A, The clone forming cell frequency (CFCF) assay was used to determine TSC number across 24 passages. Mean ± SD (n = 4 donors). B, Telomere length in TSC from normal donors. Green line indicates telomere length that is equal to that of the short telomere control, Jurkat. Red line indicates the linear regression analysis of telomere length and passage. Min-Max graphs with line at mean, box indicates 10 to 90 percentile (n = 5-9 for passages 1-7; n = 3 for passages 8-17). C, Telomere length in populations of TSC and clonal TSC isolates. Green line indicates telomere length that is equal to that of Jurkat. Min-Max graphs with line at mean, box indicates 10 to 90 percentile (n = 9 for populations; n = 7 for clones). D, Heatmap illustrating RNAseq analysis of passage 2 TSC on post-plating days 2, 3, 4, and 5 (n = 3 donors). Expression, in fragments per million reads (FPM), for telomere biology genes is shown. Background (BKG): FPM > 0.5 = above background (salmon), FPM < 0.5 below background (plum, including TERT and TERC). E, Representative flow cytometry analysis of CD151 and CD66ace expression in long-lived TSC. Live/CD49f + cells were analyzed. F, Frequency of CD151 and CD66ace within the live/CD49f + population. Changes as a function of time after plating are shown. Mean ± SEM (n = 3)

3.8 | TSC undergo secretory cell specification

Our demonstration of terminal differentiation in mouse TSC (Figures 3 and 4) coupled with our previous report that human TSC upregulated secretory cell associated genes as they were passaged,[25] suggested that human TSC underwent terminal differentiation to an airway secretory cell. Expression of secretory cell type signature genes including secretoglobins (1A1, 3A1, 3A2), mucins (5B, 5Ac), and others[33] indicates that the cell has become a club or goblet cell. Importantly, the gene products assayed in this study are cell differentiation markers and are distinct from those which define the senescence associated secretory phenotype. To further assess TSC to secretory cell differentiation, we used RNAseq to evaluate expression of the secretary cell type signature genes in P2 TSC as a function of time after plating (Figure S4). This study indicated that expression of most secretory cell signature genes increased as a function of time.

To further evaluate human TSC differentiation, we used flow cytometry to examine expression of CD151, a tetraspanin which defined a subset of human TSC[12] and CD66ace, a marker for secretory primed basal cells.[33] CD66ace + cells were a subset of the CD151+ population (Figure 7E). Although these markers defined TSC subsets (Figure 7F), their frequency did not vary over time (Figure 7F). These data suggested that accumulation of secretory-primed cells contributed to stabilization of progenitor cell frequency at later passages (Figure 7A).

3.9 | Increased proliferation and shelterin gene expression in moderate lifespan TSC

We previously used serial passage to identify TSC clones with distinct lifespans.[24] (These clones were cryopreserved at various passages for future analysis. To investigate differences among moderate (termination at p9) and long lifespan (termination at p16) TSC clones, their transcriptional profile was compared at p5 using scRNAseq. Uniform manifold approximation and projections (UMAP) identified four clusters (Figure 8A). Comparison with previously reported basal cell subtype signatures,[34] (Figure 8B) indicated that cluster-0 was composed of proliferating basal cells (basal subtype-2) and that cluster-3 contained canonical basal cells (basal subtype-1). Approximately 75% of Cluster-1 cells were secretory-primed basal cells (basal subtype-3) and 25% were β-catenin high basal cells (basal subtype-5). Cluster-2 contained a mixture of activated basal cells (basal subtype-4) as well as basal subtypes-1 and -5. Analysis of CD151 mRNA showed expression in all clusters (Figure 8C); whereas, CEACAM6 (CD66c) was limited to a subset of cluster-1 cells (Figure 8D). Expression of CEACAM1 (CD66a) and CEACAM5 (CD66e) was similar to CEACAM1 (data not shown). The frequency of CD66-expessing cells and cluster-1 was similar for the two clones (Figure 8E). The moderate lifespan clone contained more cluster-0 and cluster-3 cells and fewer cluster-2

cells than the long-lived clone (Figure 8E). These data indicate that the moderate-lifespan clone had more proliferating cells than the long lifespan clone. Analysis of telomere biology genes did not detect TERT or TERC but demonstrated upregulation of shelterin genes in the moderate lifespan clone. Collectively, these data indicate that the moderate lifespan clone, which had shorter telomeres (Figure 7), was biologically older than its counterpart and that its short telomeres were protected through upregulation of the shelterin complex genes.

3.10 | TSC number and function are decreased in DC

In contrast with TERT and TERC, our RNAseq study detected expression of telomere biology genes including DKC1, NAF1, NOT10, TERF1, TERF2, TPP1, and WRAP53 (Figure 7D) and raised the possibility that long-lived TSC used this complex to protect their relatively short telomeres. To address this question, we evaluated TSC from donors who harbor mutations in telomere biology genes, including two shelterin genes (TINF2 and CTC1). The study group contained 12 DC patients and 16 parents (Table S1). The nasal respiratory epithelium was sampled since previous studies indicated that TSC from this region were largely indistinguishable from those in other airway locations.[35,36]

Within family 1, the mother and the proband (DC patient) harbored a mutation in RTEL1. A previous study reported telomere shortening in their peripheral blood leukocytes.[37] Although the father exhibited premature aging and telomere shortening, exome sequencing did not identify a telomere biology gene mutation.[37] The parents and the proband had significantly fewer TSC than control at P1 and the proband had fewer TSC than the parents (Figure 8A). To further examine this finding, we compared TSC number in 12 DC probands and 16 parents. This study demonstrated that DC probands had fewer TSC than their adult relatives at P1 ($P = .0037$). To determine if there was a difference in telomere length in the parents relative to the proband, each parent was compared with their child (Figure 8B,C). This study showed that telomere length was significantly shorter in the proband than in the parent.

Serial passage of family 1 TSC demonstrated that TSC were depleted more rapidly in the parents and proband than in control (Figure 8A). TSC from the proband terminated at P4. Similar results were obtained for the other DC Families (data not shown). The ability of TSC from family 1 to generate functional secretory and ciliated cells was quantified at P2 using air-liquid-interface cultures. Cultures from all donors polarized and indicated that TSC were present. However, cell density and the frequency of secretory cells and ciliated cells was significantly decreased relative to control (Figure 8D-F). Similar results were obtained for additional DC families (data not shown). These data indicate that mutations in telomere biology genes, including TERT and shelterin genes, decrease TSC number and function.
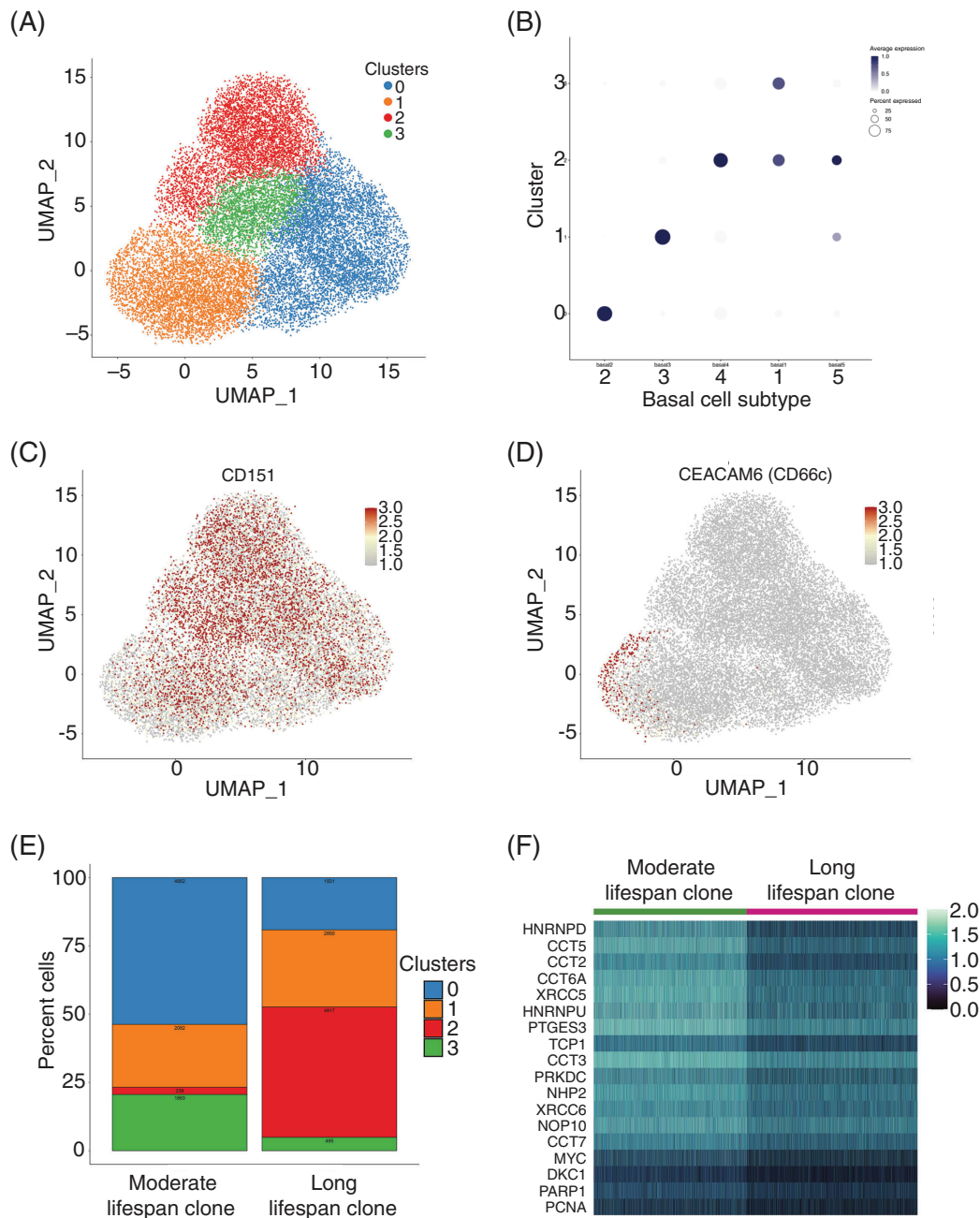
FIGURE 8 Gene expression in moderate and long lifespan human TSC clones. A, Uniform manifold approximation and projections (UMAP) were used to identity four clusters. B, Dot plot indicating the expression level and frequency of differentially expressed genes from each basal cell subtype. C, Distribution of CD151 expressing cells. D, Distribution of CEACAM6 (CD66c) expressing cells. E, Stacked column chart representing the frequency of cells in each cluster. F, Heat map representation of telomere biology gene expression

3.11 | TSC from DC patients have abnormally short telomeres

An analysis of telomere length in TSC from family 1 demonstrated that the father had significantly longer telomeres than the mother and that telomere length in TSC from the mother and the proband were similar (Figure 8G). An analysis of additional DC families demonstrated that telomeres were significantly longer the parents relative to the proband in five of six comparisons (Figure 8H). These data extend

the previously reported telomere shortening in DC-leukocytes to include airway epithelial TSC and supported the idea that shelterin genes are critical for protection of short telomeres in long-lived TSC.

4 | DISCUSSION

This study examined biological aging of TSC. Our previous study indicated that human TSC lifespan was ~40 to 50 population doublings
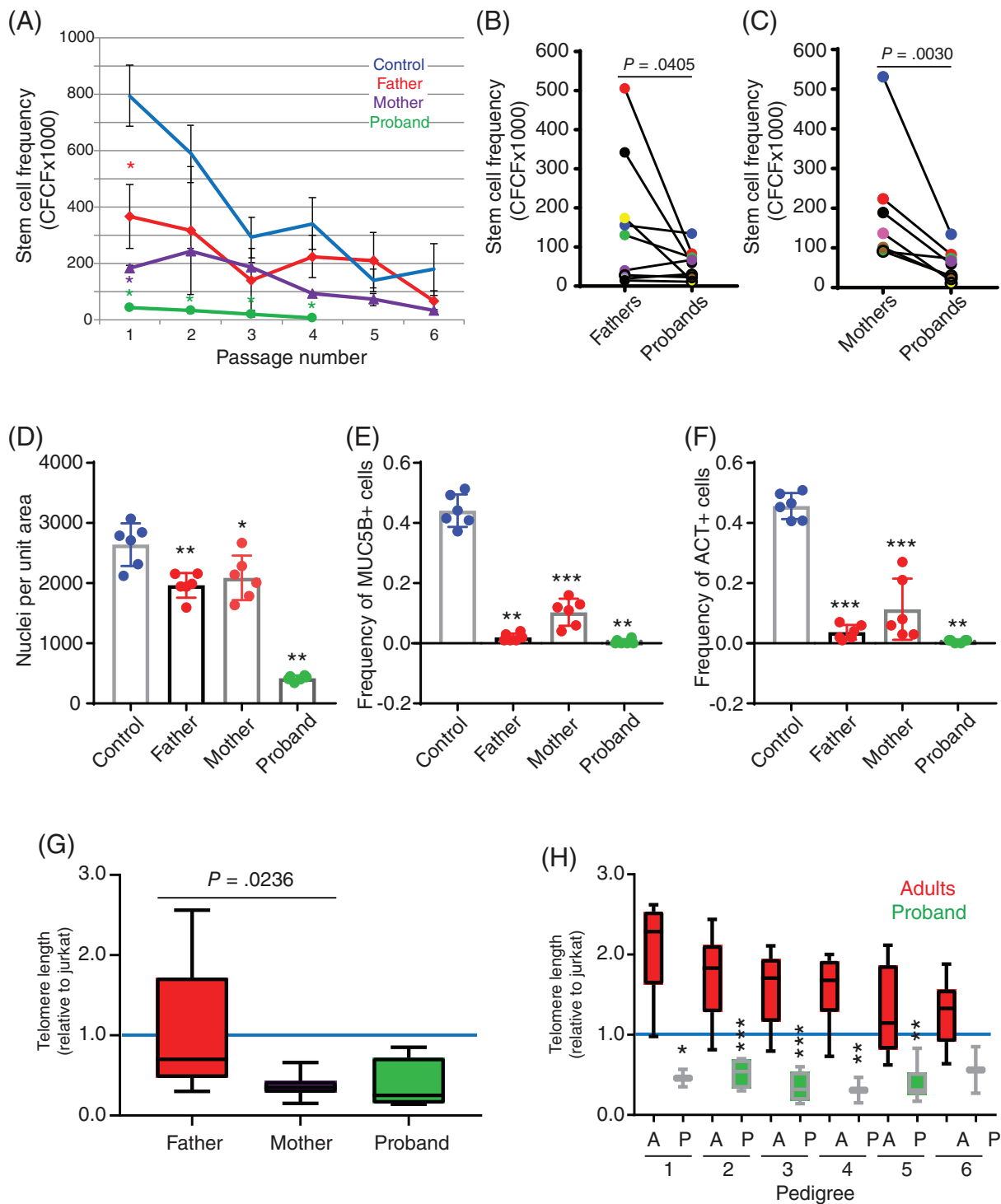
FIGURE 9 TSC number and function in dyskeratosis congenita (DC). A, The clone forming cell frequency (CFCF) assay was used to determine TSC frequency in nasal respiratory epithelial cell isolates from normal controls and in family 1 (see Table S1 for details). Red, purple, and green asterisks indicate significant differences from control (*P* < .05). Mean ± SD (n = 3 determinations/donor/timepoint). B,C, The CFCF assay was used to determine TSC frequency in nasal respiratory epithelial isolates from 12 DC families (see Table S1 for details). For clarity, the data are presented as CFCF for fathers and probands (B) or mothers and probands (C). Symbol color indicates a family and colors are consistent between panels B and C. n = 9 fathers, n = 8 mothers, n = 12 probands. D-F, TSC differentiation to functional secretory and ciliated cells was assayed via the air-liquid-interface method. D, Nuclear density as assessed by DAPI-positive cell area. E, Secretory cell differentiation as assessed by MUC5B-positive cell frequency. F, Ciliated cell differentiation as assessed by acetylated tubulin (ACT)-positive cell frequency. Mean ± SD (n = 3 replicates/donor). *P < .05, **P < .01, ***P < .001. G, Telomere length in TSC from family 1. Blue line indicates telomere length that is equal to that of the short telomere control, Jurkat. Min-Max graphs with line at mean, box indicates 10 to 90 percentile (n = 3 determinations/donor). H, Telomere length in TSC from six DC families. Blue line indicates telomere length that is equal to that of Jurkat. Min-Max graphs with line at mean, box indicates 10 to 90 percentile (n = 3 determinations/donor). *P < .05, **P < .01, ***P < .001

and that it conformed to the Hayflick limit.[38] Like stem cells from other tissues, TSC are thought to conserve their finite mitotic potential by limiting the number of times they divide. We refined this concept by showing that injury activated a fraction of the mouse TSC population[11] and suggested that this process conserved mitotic potential of the quiescent subpopulation.

We now show that activated mouse TSC continued to proliferate after the epithelium was repaired (Figure 1) and that a second injury accelerated their proliferation (Figure 2). Analysis of the TSC response to a second injury (Figures 2, 5, and 6) demonstrated activation of a new cohort of TSC which were able to regenerate the epithelium. Thus, partial activation of the TSC pool conserved the mitotic potential of the remaining TSC.

However, our analysis of mouse TSC clones also demonstrated that proliferation of activated TSC resulted in terminal differentiation (Figures 3 and 4). The majority of activated mouse TSC, 96%, did not self-renew, became UPB, and were lost from the TSC pool (Figure 4). These studies indicate that the mechanism underlying terminal differentiation was a shift from asymmetric cell division (which maintains the TSC) to symmetric cell division (which generates two UPB). Additional experiments are needed to determine if this process is unique to the terminal differentiation process and the relative contribution of intrinsic and extrinsic signals.

Collectively, our mouse clone analyses indicate that injury caused activated TSC, and possibly their supportive niche, to age at a faster rate than their nonactivated counterparts. Our analysis of secretory cell differentiation in human TSC cultures (Figure 7F,G, Figure S4) complements our analysis of terminal differentiation in mouse TSC clones. Both results indicate that generation of terminally differentiated cells squanders TSC mitotic potential. These data indicate that many injury/repair cycles decrease the reparative potential of the epithelium and that the magnitude of this decrease is dependent on the number of TSC that are activated by each injury.

Biological aging has been associated with telomere shortening and indicated cell intrinsic processes.[3] Since mice have extremely long telomeres and TERT knockout mice have complex phenotype, we analyzed telomere length in human TSC. As previously reported for postnatal somatic primary cell isolates including tissue-specific stem cells from non-pulmonary tissues,[39] our analysis showed that telomere length decreased as the cells were passaged (Figure 7) and that TSC clones had longer telomeres than the population from which they were derived. Functional significance was supported by our finding that TSC frequency was significantly decreased in DC patients relative to non-DC controls, long-lived TSC were not detected in DC patients, and TSC from DC patients had short telomeres (Figure 8). These data suggested that the TSC pool contains subpopulations that are characterized by short and long telomeres and that these subsets are comprised of biologically old and young TSC.

Our finding that human TSC frequency plateaus after passage 5 suggested the presence of an additional TSC conservation mechanism. Although some studies reported that TERT was active,[26,32] our RNAseq studies did not identify a population of TERT expressing TSC (Figure 7D, Figure S3, Figure 8). However, we did detect expression of many telomere and shelterin complex genes and our analysis of TSC from DC patients and carriers suggested that shelterin complexes may protect the relatively short telomeres found in long-lived TSC (Figure 9). Upregulation of shelterin genes in moderate lifespan TSC clones and correlation of this change with an increase in the frequency of proliferating cells (Figure 8) further supports an association between telomere length, mitotic frequency, and biological aging.

Finally, our data indicate that telomere shortening occurs as TSC divide and that differences in telomere length reflect the number of times a TSC has undergone cytokinesis. Accordingly, it is likely that freshly isolated human TSC contain subsets that are defined by the number of times they proliferated in vivo. TSC which are lost over passages 1 to 5 are likely to be cells that had proliferated many times in vivo and had expended 60% to 70% of their lifespan prior to culture. In contrast, TSC which could be passaged 15 to 20 times are likely to be a subset that proliferated fewer times in vivo and had expended only 30% to 40% of their lifespan. Thus, differences in passage-potential reflect the TSC's contribution to epithelial homeostasis and repair prior to isolation.

5 | CONCLUSION

The biological aging concept suggests that abnormal TSC function leads to airway epithelial remodeling in chronic lung disease. Our data indicate that repeated TSC proliferation results in terminal differentiation and that this process is intrinsic to the TSC. Collectively, these studies identify biological aging of TSC as a process that could drive the development of chronic lung disease.

CONFLICT OF INTEREST
B.R.S. declared research funding from Bristol Myers Squibb. The other authors declared no potential conflicts of interest.

AUTHOR CONTRIBUTIONS
M.G.: conception and design, acquisition of data, interpretation of data, manuscript preparation and review; C.L.H., A.A., S.W.L.: acquisition of laboratory data, manuscript review; D.H.: acquisition of clinical samples, manuscript review; S.W., Z.H.T., J.E.M., B.R.S.: conception and design, acquisition of data, interpretation of data, manuscript review; T.C.: conception and design, interpretation of data,

ORCID

Zhang Hong Tan https://orcid.org/0000-0003-1571-464X
Susan D. Reynolds https://orcid.org/0000-0003-4754-7858

REFERENCES

1. Barnes PJ. Senescence in COPD and its comorbidities. *Annu Rev Physiol*. 2017;79:517-539.
2. Angelidis I, Simon LM, Fernandez IE, et al. An atlas of the aging lung mapped by single cell transcriptomics and deep tissue proteomics. *Nat Commun*. 2019;10(1):963.
3. Armanios M, Blackburn EH. The telomere syndromes. *Nat Rev Genet*. 2012;13(10):693-704.
4. Jeffery PK. Remodeling in asthma and chronic obstructive lung disease. *Am J Respir Crit Care Med*. 2001;164(10 pt 2):S28-S38.
5. Whitsett JA. Airway epithelial differentiation and mucociliary clearance. *Ann Am Thorac Soc*. 2018;15(suppl 3):S143-S148.
6. Engelhardt JF, Schlossberg H, Yankaskas JR, Dudus L. Progenitor cells of the adult human airway involved in submucosal gland development. *Development*. 1995;121(7):2031-2046.
7. Hong KU, Reynolds SD, Watkins S, Fuchs E, Stripp BR. Basal cells are a multipotent progenitor capable of renewing the bronchial epithelium. *Am J Pathol*. 2004;164(2):577-588.
8. Hong KU, Reynolds SD, Watkins S, Fuchs E, Stripp BR. In vivo differentiation potential of tracheal basal cells: evidence for multipotent and unipotent subpopulations. *Am J Physiol Lung Cell Mol Physiol*. 2003;286:L643-L649.
9. Ghosh M, Brechbuhl HM, Smith RW, et al. Context-dependent differentiation of multipotential keratin 14-expressing tracheal basal cells. *Am J Respir Cell Mol Biol*. 2011;45(2):403-410.
10. Rock JR, Onaitis MW, Rawlins EL, et al. Basal cells as stem cells of the mouse trachea and human airway epithelium. *Proc Natl Acad Sci USA*. 2009;106(31):12771-12775.
11. Ghosh M, Helm KM, Smith RW, et al. A single cell functions as a tissue-specific stem cell and the in vitro niche-forming cell. *Am J Respir Cell Mol Biol*. 2011;45(3):459-469.
12. Ghosh M, Ahmad S, Jian A, et al. Human tracheobronchial basal cells. Normal versus remodeling/repairing phenotypes in vivo and in vitro. *Am J Respir Cell Mol Biol*. 2013;49(6):1127-1134.
13. Ghosh M, Smith RW, Runkle CM, Hicks DA, Helm KM, Reynolds SD. Regulation of trachebronchial tissue-specific stem cell pool size. *Stem Cells*. 2013;31(12):2767-2778.
14. Greider CW. Telomere length regulation. *Annu Rev Biochem*. 1996;65:337-365.
15. Higgs C, Crow YJ, Adams DM, et al. Understanding the evolving phenotype of vascular complications in telomere biology disorders. *Angiogenesis*. 2019;22(1):95-102.
16. Cohen BA, Turcios NL. Pulmonary manifestations of skin disorders in children. *Pediatr Clin North Am*. 2021;68(1):261-276.
17. Khincha PP, Bertuch AA, Agarwal S, et al. Pulmonary arteriovenous malformations: an uncharacterised phenotype of dyskeratosis congenita and related telomere biology disorders. *Eur Respir J*. 2017;49(1):1-6.
18. Marley SB, Lewis JL, Davidson RJ, et al. Evidence for a continuous decline in haemopoietic cell function from birth: application to evaluating bone marrow failure in children. *Br J Haematol*. 1999;106(1):162-166.
19. Cole BB, Smith RW, Jenkins KM, Graham BB, Reynolds PR, Reynolds SD. Tracheal basal cells: a facultative progenitor cell pool. *Am J Pathol*. 2010;177(1):362-376.
20. Tumbar T, Guasch G, Greco V, et al. Defining the epithelial stem cell niche in skin. *Science*. 2004;303(5656):359-363.
21. Diamond I, Owolabi T, Marco M, Lam C, Glick A. Conditional gene expression in the epidermis of transgenic mice using the tetracycline-regulated transactivators tTA and rTA linked to the keratin 5 promoter. *J Invest Dermatol*. 2000;115(5):788-794.
22. Smith RW, Hicks DA, Reynolds SD. Roles for beta-catenin and doxycycline in the regulation of respiratory epithelial cell frequency and function. *Am J Respir Cell Mol Biol*. 2012;46(1):115-124.
23. You Y, Richer EJ, Huang T, Brody SL. Growth and differentiation of mouse tracheal epithelial cells: selection of a proliferative population. *Am J Physiol Lung Cell Mol Physiol*. 2002;283(6):L1315-L1321.
24. Hayes D Jr, Kopp BT, Hill CL, et al. Cell therapy for cystic fibrosis lung disease: regenerative basal cell amplification. *Stem Cells Translational Medicine*. 2019;8:225-235.
25. Reynolds SD, Rios C, Wesolowska-Andersen A, et al. Airway progenitor clone formation is enhanced by Y-27632-dependent changes in the transcriptome. *Am J Respir Cell Mol Biol*. 2016;55:323-336.
26. Suprynowicz FA, Upadhyay G, Krawczyk E, et al. Conditionally reprogrammed cells represent a stem-like state of adult epithelial cells. *Proc Natl Acad Sci USA*. 2012;109(49):20035-20040.
27. O'Callaghan N, Dhillon V, Thomas P, Fenech M. A quantitative real-time PCR method for absolute telomere length. *Biotechniques*. 2008;44(6):807-809.
28. Hsieh AYY, Saberi S, Ajaykumar A, et al. Optimization of a relative telomere length assay by monochromatic multiplex real-time quantitative PCR on the LightCycler 480: sources of variability and quality control considerations. *J Mol Diagn*. 2016;18(3):425-437.
29. Blanpain C, Lowry WE, Geoghegan A, Polak L, Fuchs E. Self-renewal, multipotency, and the existence of two cell populations within an epithelial stem cell niche. *Cell*. 2004;118(5):635-648.
30. Goodell MA, Rosenzweig M, Kim H, et al. Dye efflux studies suggest that hematopoietic stem cells expressing low or undetectable levels of CD34 antigen exist in multiple species. *Nat Med*. 1997;3(12):1337-1345.
31. Mou H, Vinarsky V, Tata PR, et al. Dual SMAD signaling inhibition enables long-term expansion of diverse epithelial basal cells. *Cell Stem Cell*. 2016;19(2):217-231.
32. Yim HW, Slebos RJ, Randell SH, et al. Smoking is associated with increased telomerase activity in short-term cultures of human bronchial epithelial cells. *Cancer Lett*. 2007;246(1–2):24-33.
33. Carraro G, Mulay A, Yao C, et al. Single cell reconstruction of human basal cell diversity in normal and IPF lung. *Am J Respir Crit Care Med*. 2020;202:1540-1550.
34. Carraro G, Langerman J, Sabri S, et al. Transcriptional analysis of cystic fibrosis airways at single-cell resolution reveals altered epithelial cell states and composition. *Nat Med*. 2021;27(5):806-814.
35. Boudewijn IM, Faiz A, Steiling K, et al. Nasal gene expression differentiates COPD from controls and overlaps bronchial gene expression. *Respir Res*. 2017;18(1):213.
36. Wesolowska-Andersen A, Everman JL, Davidson R, et al. Dual RNA-seq reveals viral infections in asthmatic children without respiratory illness which are associated with changes in the airway transcriptome. *Genome Biol*. 2017;18(1):12.
37. Ballew BJ, Yeager M, Jacobs K, et al. Germline mutations of regulator of telomere elongation helicase 1, RTEL1, in dyskeratosis congenita. *Hum Genet*. 2013;132(4):473-480.
38. Hayflick L. The cell biology of aging. *J Invest Dermatol*. 1979;73(1):8-14.

39. Bessler M, Wilson DB, Mason PJ. Dyskeratosis congenita. *FEBS Lett*. 2010;584(17):3831-3838.

SUPPORTING INFORMATION

Additional supporting information may be found in the online version of the article at the publisher's website.